Understanding the Optical Properties of Au@Ag Bimetallic Nanoclusters Through Time-Resolved and Nonlinear Spectroscopy

Rosina Ho-Wu,^a Prabhat Kumar Sahu,^a Nancy Wu,^a Tian Kai Chen,^b Carrie Yu,^a Jianping Xie,^b Theodore Goodson III^{*a}

^aDepartment of Chemistry, University of Michigan, Ann Arbor, Michigan 48109, USA

^bDepartment of Chemical and Biomolecular Engineering, National University of

Singapore, 4 Engineering Drive 4, 117576, Singapore

I. Abstract

Bimetallic Au@Ag nanoclusters have been shown to possess unique properties compared to their monometallic Au or Ag nanoclusters. In the present work, the optical properties of three bimetallic nanoclusters namely Au₁₅@Ag, Au₁₈@Ag and Au₂₅@Ag have been investigated by steady state and time-resolved absorption and emission, and two-photon absorption measurements. The nanoclusters are composed of a gold core and an alternating Au-Ag-ligand surface shell structure. We observed that the absorption and emission of the bimetallic Au@Ag nanoclusters are enhanced compared to the pure Au nanoclusters; the emission is, additionally, blue-shifted. All of the mixed clusters showed impressive twophoton absorption coefficients with Au25@Ag showing a largely enhanced effect. The excited state dynamics of the Au@Ag nanoclusters were studied by time-resolved transient absorption and emission which show that the bimetallic nanoclusters have longer excited state lifetimes than the Au nanoclusters. Specifically, the surface-related excited states showed a larger increase in lifetime than the core-related states, which indicates Ag binding on the staple motifs of the Au nanoclusters. This spectroscopic evidence shows that the bimetallic nanoclusters have gained significant Ag character, and that the Ag atoms bind on the staple motifs.

II. INTRODUCTION

There is great interest in metal nanoclusters which are quantum sized (< 2 nm) nanoparticles with molecular-like properties.^{1–3} Recently, research effort has been devoted to the understanding of the fundamental science behind these nanoclusters.^{4–7} In particular, the structure-function relationship which governs the transition from metal particle (surface

plasmon) behavior to molecular behavior has been a question of scientific importance.^{2,8–10} Since there are large differences in the structure between different metal nanoclusters, a direct understanding of the size-property correlation is challenging.⁸ Jin et al. has taken the first detailed step in understanding the size-property evolution of a magic cluster series of Au.² The challenge still remains to encompass all the known stable sized nanoclusters into a bigger size-property picture.² On the other hand, the structure-property relationship is now better understood due to the successful crystallization of metal nanoclusters and structural determination, and the combined experimental and theoretical studies of their electronic properties.^{3,10–12} It is known, for example, that the electronic transitions in Au₂₅(SR)₁₈ nanoclusters are due to the intra-bands and inter-bands transition of the Au₁₃ icosahedral core.^{11,13,14} Ultrafast spectroscopic techniques allow us to understand the intra-molecular energy transfer property and the origin of fluorescence of gold and silver metal nanoclusters.^{3,10,15–18}

Two of the molecular-like properties of metal nanoclusters that are most interesting for applications are fluorescence and two-photon absorption (TPA). 19-23 They have found applications in bioimaging, 24-27 sensing, 28-31 and catalysis. 32-34 However, the fluorescence quantum yields of some metal nanoclusters are low.³⁵⁻³⁸ Motivated by the useful applications of nanocluster's fluorescence, synthetic efforts have been focused on preparing highly fluorescent metal nanoclusters. 9,35-37,39-41 One important discovery is the phenomenon of aggregation-induced emission (AIE) of the precursors of gold nanoclusters, Au(I)thiolates.³⁵ Later, Xie et al.³⁷ expanded this discovery to bimetallic gold-silver nanoclusters. Silver nanoclusters are known to show enhanced optical properties when compared to gold nanoclusters, however, due to their lower colloidal stability, they have yet to receive the same research interest as gold nanoclusters. 9,10,42 Nevertheless, silver has been used as a dopant in gold nanoclusters and the resulting bimetallic nanoclusters have shown synergistic effects from the two metal atoms. 43 Previous reports of the highly fluorescent Au@Ag nanoclusters show that the silver ions do not replace the gold atoms, but rather, they bind to the sulfur atoms at the gold nanocluster's surface.³⁷ However, the characterization of the Au@Ag nanoclusters shows a distribution of 1 to 7 silver ions for each of the three nanoclusters, Au₁₅, Au₁₈ and Au₂₅, which are treated as spherical particles.³⁷

In this contribution, enhanced fluorescence properties of Ag nanoclusters are combined with the stability of Au nanoclusters. Ag ions are integrated into the ligand of gold nanoclusters, by binding onto sulfur, resulting in a unique stable bimetallic cluster that exhibits enhanced fluorescence properties. We have investigated the optical properties of three bimetallic nanoclusters with nonlinear optical and time-resolved measurements. The results are compared with their monometallic counterpart and discussed with respect to the structures of the bimetallic nanoclusters.

III. EXPERIMENTAL SECTION

A. Materials. All chemicals were used as received: hydrogen tetrachloroaurate(III) trihydride (HAuCl₄·3H₂O), silver nitrate (AgNO₃), and L-glutathione reduced (GSH) were purchased from Sigma-Aldrich; Sodium hydroxide (NaOH) was purchased from Merck; Carbon monoxide (CO, 99.9%) was purchased from Singapore Oxygen Air Pte Ltd (SOXAL). Ultrapure water (18.2 M Ω ·cm) was used to prepare the aqueous solutions. All glassware was washed with aqua regia and rinsed with ethanol and ultrapure water before use.

B. Synthesis of Au and Au@Ag bimetallic nanoclusters. The Au₁₅(GSH)₁₃, Au₁₈(GSH)₁₄, Au₂₅(GSH)₁₈ and the Au@Ag nanoclusters were synthesized according to published method.²⁶ To prepare Au₁₅(GSH)₁₃, Au₁₈(GSH)₁₄, and Au₂₅(GSH)₁₈, 0.5 mL of 20 mM HAuCl₄ solution was mixed with 0.4 mL of 50 mM GSH solution. After 2 min, 1 M NaOH solution was added to bring up the pH of solutions. The pH was brought to 9, 10, and 11 for the preparation of Au₁₅(GSH)₁₃, Au₁₈(GSH)₁₄, and Au₂₅(GSH)₁₈, respectively. The reaction solutions were bubbled with 1 bar of CO for 2 min, and the reactions were allowed for additional 24 hours airtightly. The as-synthesized Au nanoclusters were then purified by dialysis for about 9 hours using a dialysis bag with 3000 Da molecular weight cut-off (MWCO). After that, 0.5 mL of 2 mM AgNO₃ solution was added to 5 mL of purified Au₁₅(GSH)₁₃, Au₁₈(GSH)₁₄, and Au₂₅(GSH)₁₈ solutions under 1000 rpm stirring and the reactions proceeded for 15 min, yielding Au₁₅@Ag, Au₁₈@Ag, and Au₂₅@Ag nanoclusters, respectively.

- C. Steady-state absorption and emission measurements. UV-visible absorption spectra of the nanoclusters were obtained using an Agilent 8453 Spectrophotometer over the range of 250-1100 nm. The solutions of the nanoclusters were prepared in nanopure water at 2.5 mL volume which resulted in different concentrations of the nanoclusters ($35 59 \mu M$). Steady-state emission spectra were collected using Fluoromax-2 fluorimeter from Horiba at 400 nm excitation. All measurements were collected using a 1-cm cuvette.
- **D. Emission quantum yield measurements.** Emission measurements were collected using a Hamamatsu photomultiplier tube coupled to a monochromator. An excitation of 400 nm was used by frequency doubling of an 800 nm output from a Kapteyn-Murnane Ti:sapphire laser. The emission was collected over the range of 420 750 nm. For each nanocluster, an emission maximum was observed at 500 nm. The area under the emission peak was integrated to calculate the relative quantum yield in reference to a dilute coumarin 30 solution in methanol ($\Phi = 0.67$).
- **E. Two-photon excited fluorescence measurements.** A mode-locked Ti:Sapphire laser (Kapteyn-Murnane) was used to conduct two-photon absorption (TPA) cross section measurements. The intensity of the 800nm output beam for excitation was controlled using a neutral density filter. The fluorescence of the nanoclusters was collected perpendicular to the excitation beam by a photomultiplier tube (Hamamatsu) coupled to a monochromator. Two-photon excited fluorescence was recorded over the range 420 850 nm. A dilute coumarin 30 solution in methanol ($\sigma = 0.33$ GM) was used as the standard.
- **F. Time-resolved fluorescence measurements.** The fluorescence decay kinetics of the nanoclusters were observed at 500 nm and 650 nm using the time-correlated single photon counting method. A diode-pumped Ti:sapphire laser was used to produce the fundamental wavelength of 800 nm. This output was frequency doubled to 400 nm using a β -barium borate crystal. The excitation beam was directed to a focusing lens (f = 11.5 cm) and then on the sample cuvette. The fluorescence was collected perpendicular to the excitation beam, using a monochromator and photomultiplier tube. Repetition rate of the pulses was set to 383 kHz. Time resolution to 1 ns is limited by the time to amplitude converter.
- **G. Femtosecond transient absorption measurements.** The pump-probe experiments were performed with an amplified laser system by Spectra-Physics Spitfire. The amplified laser has a pulse duration of ~100 fs and a repetition rate of 1 kHz. The output of a 800 nm beam

(800 mW) was split into 85% for the pump and 15% for the probe. The pump beam (400 nm) was obtained by second harmonic generation with a BBO crystal, chopped at 100 Hz and focused on the 1 mm sample cell. The probe beam was directed into a delay line and focused on a sapphire plate to generate a broadband white light. The probe beam was focused and overlapped with the pump beam. The probe beam was then focused on the CCD detector (Ocean Optics). Data acquisition software is Helios, and data analysis software is Surface Xplorer Pro, both of which are from Ultrafast Systems, Inc.

H. Nanosecond transient absorption measurements. For the nanosecond transient absorption measurements consists of Lab Series 170 neodymium-doped yttrium aluminium garnet (Nd:YAG) Quanta-Ray (Spectra Physics) laser. LP980 (Edinburg) spectrometer has been used for the data collection device and probe source. A xenon lamp within the LP980 is used as a broadband light source to probe the excited state. The probe pulse is perpendicular to the laser excitation. This geometry is helpful in getting information about the transient species which only occur in the overlapped region while minimizing scattering, fluorescence, triplet-triplet annihilation and photodegradation. A PMT (Hamamatsu R928) is used to detect the signal at right angle to the excitation beam. The electrical signals are measured by a TDS3052B Model oscilloscope which is connected to the PMT. The electrical signal is converted into change of optical density (ΔOD) by L900 software. The data are analyzed through the same software.

IV. RESULTS AND DISCUSSION

A. Structures of the bimetallic metal nanoclusters

As mentioned above the bimetallic Au@Ag nanoclusters were synthesized by the addition of Ag⁺ to the nanoclusters in a 1-to-4 molar ratio of Ag⁺-to-nanocluster.³⁷ Unlike other bimetallic Au/Ag nanoclusters,⁴³ the Ag⁺ ions bind to the S atoms of the S-Au-S staple motifs of the parental Au nanoclusters.³⁷ In previous studies, the addition of metal cations to metal nanoclusters produced metal-exchanged bimetallic nanoclusters.⁴⁴ The difference in the reaction product may be due to the lower molar ratio of Ag⁺-to-nanocluster and the lack of extra ligands to perform surface motif exchange reactions.^{37, 44-46} Based on MALDI mass spectrometry and ICP experiments, it was determined that the Au@Ag nanoclusters can have 1 to 7 Ag atoms.³⁷ Herein, we examined the possible Ag⁺ binding sites on the Au

nanoclusters based on the reported structures of $Au_{15}(SR)_{13}$, $Au_{18}(SR)_{14}$, and Au₂₅(SR)₁₈. ^{11,47-49} The Au₁₅ nanocluster is the smallest stable thiolate-protected Au nanocluster that was synthesized and characterized. The Au₁₅ nanocluster has a 4-atom Au core arranged in a tetrahedral, and 11 Au atoms distributed as S-Au-S motifs on the surface. Jiang⁴⁷ and Tlahuice-Flores⁵⁰ have independently proposed two different arrangements of these 11 surface Au atoms. The structure shown in Figure 1 is based on Jiang's Au₁₅ nanocluster structure which features two Au₃S₄ trimer motifs and one Au₅S₅ pentamer ring interlocking one of the trimers on the surface of the Au₄ core.⁵¹ The bond length of Ag-S varies between Ag nanoclusters. 42,51 Considering a bond length of ~2.6 Å, and a bond length of ~2.9 Å between Ag-Au, 40 it appears that inter-staple binding of Ag+ is the most likely option as intra-staple binding would result in a very short Ag-Au distance (~1.3 Å). Since S can have up to 4 covalent bonds, there are 5 possible binding sites for Ag⁺ in the Au₁₅(GSH)₁₃ nanocluster (Figure 1). Each of the 5 binding sites corresponds to the interstaple binding of the Au₅S₅ pentamer ring with one of the S atoms of the Au₃S₄ motif via S-Ag-S binding (Figure 1). One of the S atoms in the pentamer ring can form inter-staple binding with either S atoms (in the trimer motif) that are furthest from the Au core. The Ag⁺ that forms this inter-staple binding is labeled A and B in Figure 1, which constitute two structural isomers for Au₁₅@Ag nanoclusters. The metal atoms in this nanocluster can be divided into three categories: core Au atoms, surface Au atoms and surface Ag atoms. The core-surface-Ag ratio for Au₁₅@Ag nanocluster is, therefore, 4-11-5 (or 1-2.7-1.2).

Similarly, inter-staple binding of Ag⁺ is expected in Au₁₈@Ag and Au₂₅@Ag nanoclusters. In the Au₁₈(SR)₁₄ nanocluster, 3 monomeric AuS₂ motifs bind between opposite vertexes of the fused octahedral Au₉ core.^{48,49} The possible inter-staple bindings of Ag⁺ are between the monomeric AuS₂ and the dimeric Au₂S₃, and between AuS₂ and the tetrameric Au₄S₅ motif (Figure 1). Therefore, 5 inter-staple bindings of Ag⁺ are possible in the Au₁₈@Ag nanocluster. The core-surface-Ag ratio of the Au₁₈@Ag nanocluster is 9-9-5 (or 1-1-0.6). The structure of the Au₂₅(GSH)₁₈ nanocluster is more symmetrical compared to Au₁₅(GSH)₁₃ and Au₁₈(GSH)₁₄, featuring 6 dimeric Au₂S₃ motifs that bind to the Au₁₃ core in a three perpendicular planes fashion.^{11,14} Due to the more symmetric arrangement of the staple motifs on the Au₂₅(GSH)₁₈ nanocluster, up to 6 Ag⁺ can form inter-staple bindings with the 6 staple motifs (Figure 1). The Au₂₅@Ag nanocluster shown in Figure 1 represents

the most symmetric arrangement of the 6 Ag^+ on the nanocluster's motifs, It is also possible that the Ag-3 and the Ag-6 can both be placed on the same side of the nanocluster instead of being placed on opposite sides as shown. The proposed $Au_{25}@Ag$ nanocluster structure has a core-surface-Ag ratio of 13-12-6 (or 1-0.9-0.5).

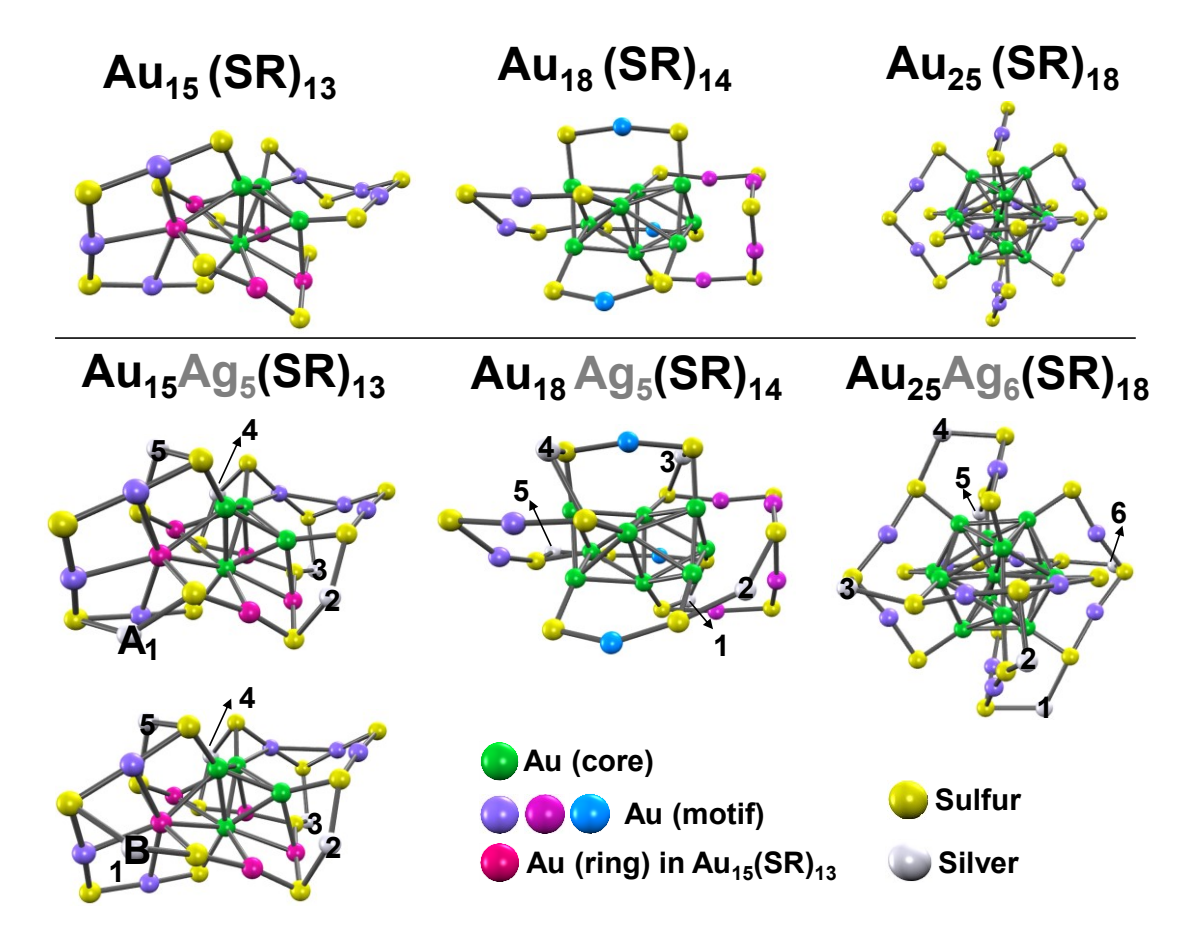


Figure 1. The structures of the parental Au nanoclusters, Au_{15} , 50 Au_{18} , 64 and Au_{25} , 11 and the structures of the Au@Ag nanoclusters. The ligand, -R group, is omitted for clarity.

B. Linear Absorption spectra

Shown in Figure 2 are the linear absorption spectra for the investigated clusters. Optical absorption of gold nanoclusters show mainly sp \leftarrow d and sp \leftarrow sp transitions of the gold atoms.³ However, the Kohn-Sham orbital energy level diagrams of the gold nanoclusters show that there are significant contribution from the sulfurs' 3p orbital.^{11,48} In a theoretical study of silver-doped Au₂₅(SH)₁₈ nanoclusters, the optical absorption spectra of Au_{25-x}Ag_x

nanoclusters exhibit a shift to higher energy with increasing Ag-to-Au ratio.⁵² The theoretical absorption spectra were modeled after a Au_{25-x}Ag_x structure where the Ag atoms occupy the icosahedra shell positions. In the experimental absorption spectra nanoclusters (Figure 2), all the Au@Ag nanoclusters under investigation, showed absorption peak at 350 nm and 470 nm, similar to the pure Au nanoclusters. The only difference that is observed is an increase in the absorption coefficient compared to the parental Au nanoclusters. For the Au@Ag nanoclusters, the peaks at 350 nm and 470 nm become more pronounced. Therefore, the Ag⁺ should be occupying in the staple motifs positions on the Au nanoclusters as there is not significant shifts in the absorption spectra that indicates Ag doping on the Au nanocluster's core. The additional d orbitals from Ag⁺ possibly contributes to the increase in the absorption coefficient of the nanoclusters. The increase in the absorption coefficient is more significant in the two smaller nanoclusters, Au₁₅@Ag and Au₁₈@Ag due to the higher Ag-to-Au (core) atom ratio.

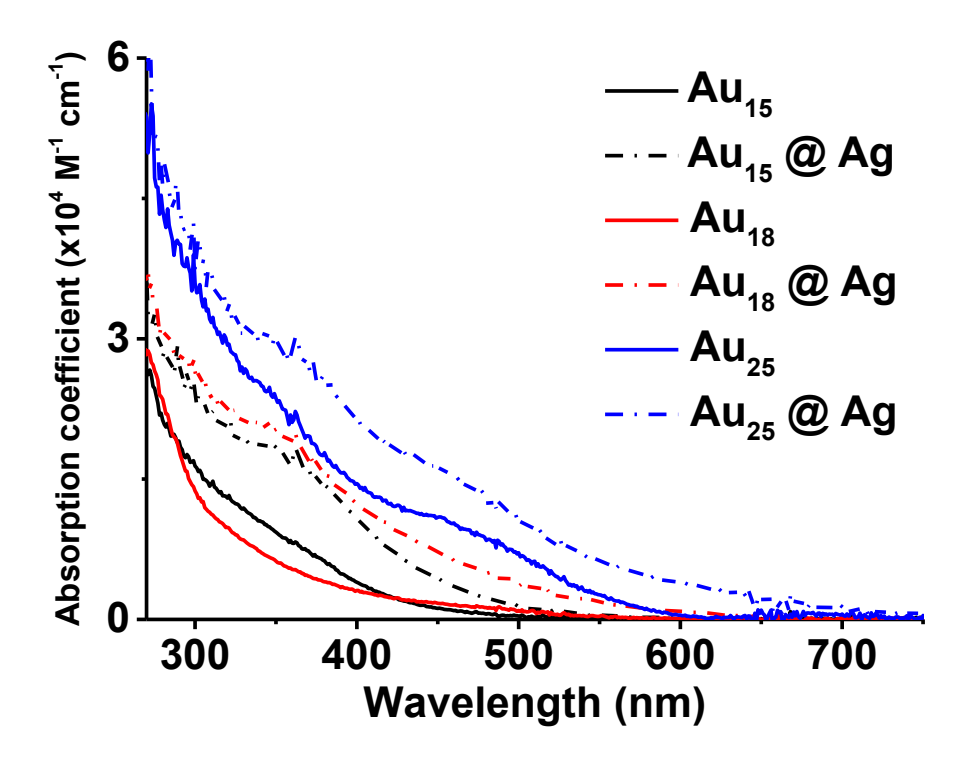


Figure 2. Steady state absorption of Au and Au@Ag nanoclusters.

C. Emission spectra

Shown in Figure 3 are the normalized emission spectra for the investigated clusters. The steady state emission intensities of the Au@Ag nanoclusters were observed to be higher than

their Au counterpart (Figure S1). The near-IR emission of gold nanoclusters was found to originate from the [Au_xSR_y]_n staple motifs, or surface excited states, by energy transfer from the core excited states. 15,17,38 This emission is stronger than the core excited states emission by approximately 4 orders of magnitude.^{38,53} The emission of gold nanoclusters is typically broad and the emission maxima can vary between 700 to 1,000 nm depending on the type of ligand. 38,41,54,55 Silver nanoclusters, on the other hand, exhibit fluorescence at wavelengths less than 700 nm. 9,10,16,42 The emission peaks of the Au@Ag nanoclusters clearly shift towards 650 nm which gives evidence that the staple motifs of the nanoclusters have more silver character. In other words, due to the higher fluorescence efficiency of silver nanoclusters, the newly formed S-Ag-S at the staple motifs of the Au nanoclusters masks the fluorescence that originates from the S-Au-S staples. It is observed that the spectra shift is greater in the smaller nanocluster, due to the higher ratio of staple motif metal atoms (both Au and Ag) than core Au metal atoms. The emission quantum yield (QY) enhancement factor was previously determined to be 84 for Au₁₅@Ag, 18 for Au₁₈@Ag and 27 for Au₂₅@Ag compared to their parental Au nanoclusters.³⁷ Not only did the Au₁₅@Ag nanocluster show the largest emission blue shift, but also the largest emission quantum yield enhancement which indicates a significant Ag character in this bimetallic nanocluster.

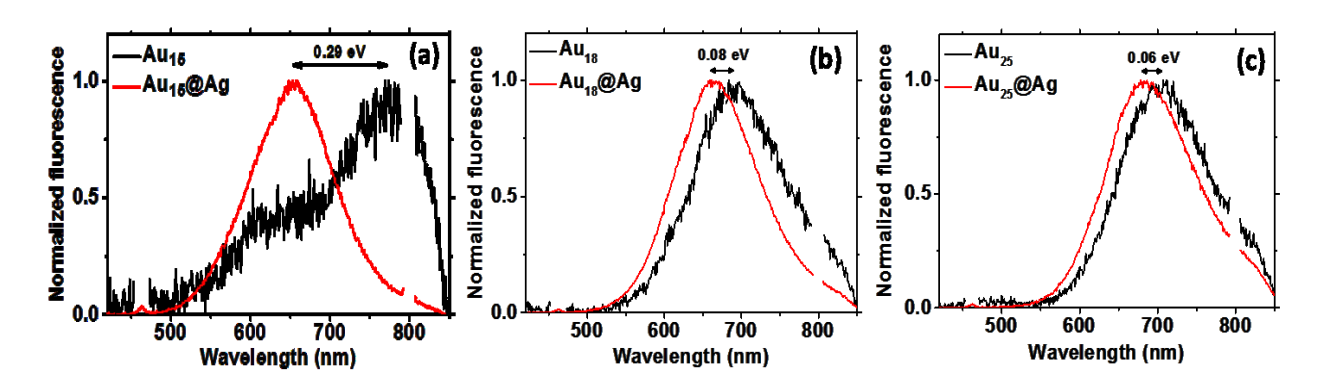


Figure 3. Normalized steady state emission spectra of (a) Au_{15} and $Au_{15}@Ag$, (b) Au_{18} and $Au_{18}@Ag$ and (c) Au_{25} and $Au_{25}@Ag$ nanoclusters.

D. Time-resolved fluorescence measurements

Time-resolved fluorescence spectroscopic methods have been used to rigorously study the fluorescence processes of metal nanoclusters. Metal nanoclusters are categorized by their well-defined structure and their size-specific fluorescence properties which resemble molecular fluorescence due to quantum confinement. S6-61 It has been found that nanoclusters exhibit fluorescence from both the core and surface states. The surface state is composed of metal-ligand motifs which stabilize the metal core. 11,42-43,47,62 Due to a separate emission from the surface states, the fluorescence kinetics of metal nanoclusters is further characterized by the composition of its ligands. 38,63

Similar to the steady state emission, the time-resolved fluorescence emission of the Au@Ag nanoclusters shows an enhancement in surface state emission (650 nm) compared to their parent counterpart. The core emission lifetimes, measured at 500 nm, for all the nanoclusters are also provided in Table 1. Au₁₅@Ag exhibited a core emission lifetime of which is longer than that observed for Au₁₅. Au₁₈ also exhibited increased fluorescence emission lifetime when Ag was added. Au₂₅, on the other hand, displayed the same emission lifetime when the Ag was added into the staple motifs. Relating to the surface state emission lifetimes, it is observed in Figure 4A and Table 1 that Au₁₅@Ag has a 4.4 times increase compared to that of Au₁₅. However, the surface state emission lifetimes of Au₁₈ and Au₁₈@Ag does not show any appreciable difference. Likewise, the surface state emission lifetimes of Au₂₅@Ag and Au₂₅ show negligible difference. Consistent with the steady state results, the time-resolved emissions show that the smallest nanocluster in this investigation has more Ag character compared to the other two bimetallic nanoclusters. The Au@Ag nanoclusters showed similar core states emission lifetime, indicating that the core-related states of the Au nanoclusters are minimally affected by the Ag binding on the surface's staples. Multiple studies that alter the conditions of nanoclusters have been carried out to explore the fluorescence lifetimes.^{29, 64-65, 66} The effects of changing the ligands on the Au clusters were shown to increase lifetimes if the ligands contained electron rich groups and atoms with strong electron donating capabilities due to ligand to metal complex charge transfer.63 Tang et al. have shown that the addition of metal cations like Hg2+ serve as a fluorescence quencher to the long decay component of the BSA-protected Au₂₅ nanocluster.66 Increasing concentration of Hg2+ resulted in decreasing fluorescence lifetimes. Hg²⁺, with a d¹⁰ electronic structure, interacts with the triplet state electrons in the

ligand surface Au(I)-S semirings resulting in an electron transfer from Au₂₅ nanocluster to Hg^{2+} .⁶⁶⁻ However, it is important to note that these metal ions are not integrated into the structure of the metal-ligand surface layer of the nanocluster.

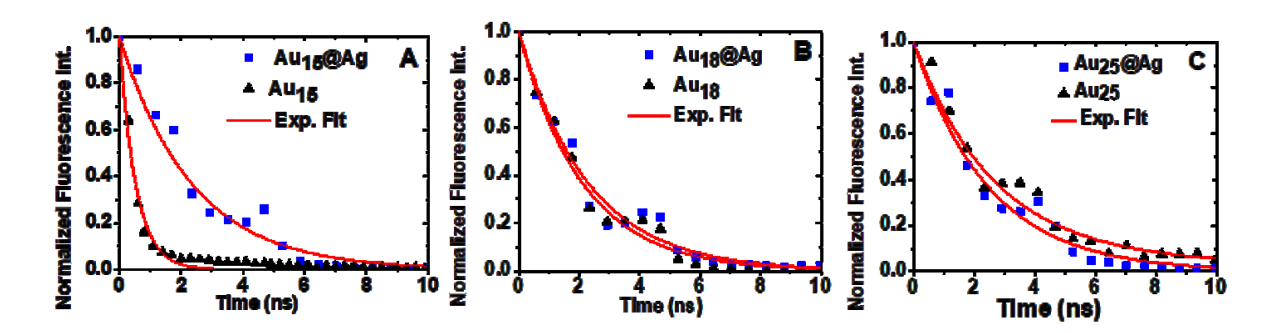


Figure 4. Normalized fluorescence decays of Au and Au@Ag nanoclusters at monitoring wavelength 650 nm. (A) Au₁₅ and Au₁₅@Ag, (B) Au₁₈ and Au₁₈@Ag and (C) Au₂₅ and Au₂₅@Ag.

Table 1. Fluorescence lifetimes of core (500 nm) and surface state (650 nm) emissions.

Sample Name	τ(ns) at 500nm	τ(ns) at 650nm
Au ₁₅	3.53±0.18	0.53±0.03
Au ₁₅ @Ag	4.95±0.25	2.35±0.12
Au ₁₈	4.19±0.21	2.11±0.11
Au ₁₈ @Ag	5.88±0.29	2.30±0.12
Au ₂₅	4.48±0.22	2.62±0.13
Au ₂₅ @Ag	3.62±0.18	2.47±0.12

E. Two-photon fluorescence of the bimetallic clusters

The Au@Ag nanoclusters showed two-photon excited fluorescence as shown by the intensity dependence plots which show slopes of 2 (Figure 5). The TPA cross sections of the nanoclusters were determined at 500 nm emission. For determining TPA cross section, previously reported values of fluorescence quantum yields of the bimetallic nanoclusters ³⁷

have been used (Table 2). Recently, Yau et. al. have reported the TPA cross sections of Ag₁₅(SG)₁₁ and Ag₃₂(SG)₁₉.¹⁰ Despite its higher fluorescence quantum yield and molar absorption coefficient, the TPA crossection of Ag₁₅(SG)₁₁ have been shown to be four orders of magnitude lower compared to Au nanoclusters due to fewer d orbital electrons in Ag.^{10,16,67} Furthermore, Ag₃₂, did not show two-photon excited fluorescence which the authors have reasoned towards a rapid internal conversion to be detectable by two photon excited fluorescence.¹⁰

Although the Au₁₅@Ag nanocluster showed the largest steady state absorption and emission enhancement, its TPA cross section remain similar to that of the Au₁₅ nanocluster (Table 2). The Au₁₈@Ag nanocluster showed a decrease in the TPA cross section by a factor of 0.5. The Au₂₅ nanocluster has the most symmetric structure out of the three nanoclusters; a symmetry which is retained also in the bimetallic Au₂₅@Ag nanocluster. The Au₂₅@Ag nanocluster is also the only bimetallic nanocluster that showed TPA cross section enhancement. High symmetry in molecular systems has been shown to also possess a higher TPA cross section due to the enhancement in the excited state dipole moment. ⁶⁸ Taking into account the number of metal atoms, the TPA cross sections per atom were obtained for comparison. The TPA cross sections per atom of the Au@Ag nanoclusters were calculated based on 5 Ag atoms for Au₁₅ and Au₁₈ and 6 Ag atoms for Au₂₅ nanoclusters. The enhancement factor of the TPA cross sections per atom remained similar between Au and Au@Ag nanoclusters since the number of Ag atoms does not vary significantly between the three different nanocluster sizes.

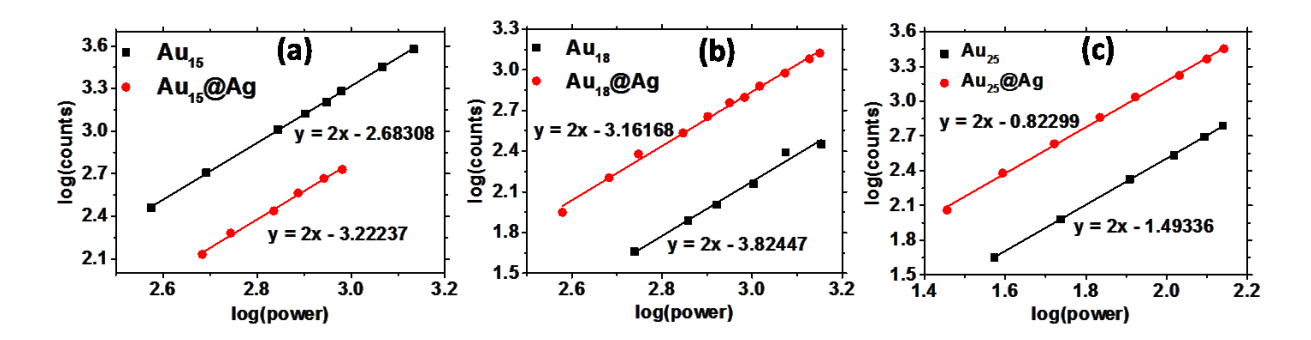


Figure 5. Intensity-dependent two-photon excited fluorescence of Au and Au@Ag nanoclusters.

Table 2. Relative TPA cross sections of Au and Au@Ag nanoclusters.

	Au NC			Au@Ag NC		Enhancement factor		
	QY(%) ^a	δ (GM)	δ/atom (GM)	QY(%) ^a	δ (GM)	δ/atom (GM)	δ	δ/atom
Au ₁₅	0.025	2,000	133	2.1	1,900	95	0.9	0.7
Au ₁₈	0.37	7,400	411	6.8	3,900	169	0.5	0.4
Au ₂₅	0.12	427,000	17,080	3.2	888,000	28,645	2	1.7

^aValues are reported from reference 37.

F. Transient absorption spectroscopy of the bimetallic clusters

The physical evolution of the excited states of gold nanoclusters in the femtosecond regime has been studied in detail.^{3,15,17} Using time-resolved fluorescence upconversion, the core emission of Au₅₅ was measured with a reported decay constant of 250 fs.¹⁵ This fast decay was attributed to the filling of the ground state hole, created by excitation, via a different electron in the higher energetic state, similar to the Auger recombination process of nanoparticles.⁶⁹ This process is measured through the emission from the higher excited state whereas the lower energy excited state results in a non-radiative decay process. The longer NIR emitting surface state of Au₅₅ is formed through an energy transfer from the lowest excited state to the surface state. The existence of the long decay component of the Au₅₅ nanocluster was attributed to an energy transfer from the core Au electrons to the electrons of the Au occupying the ligand shell.

The excited state dynamics of the Au@Ag nanoclusters were examined by femtosecond and nanosecond transient absorption spectroscopy. Excitation in excess of the HOMO-LUMO gap was chosen at 400 nm, and the excited state dynamics were probed with a broadband white light. The transient absorption of the Au25 and Au25@Ag nanoclusters show similar peak positions in the excited state absorption (Figure 6c and 6d). The Au15@Ag nanocluster, on the other hand, shows a small blue shift in the excited state absorption peak position which indicates significant Ag contribution on the surface staple of the Au15@Ag nanocluster (Figure 6). The femtosecond transient kinetic of the Au and

Au@Ag nanoclusters show a long core excited state (indicated as "inf" in Table 3 and 4) that does not decay within the measured time frame (1 ns) (Table 3 and 4). The surface-related states at ~600 nm show an initial fast ground state bleach (GSB), followed by an excited state absorption (ESA). Overall, the excited state behavior between the Au and the Au@Ag nanoclusters is similar, but the transient absorption of the bimetallic nanoclusters is stronger than the parental Au nanocluster. This observation is also made in the steady state absorption, which indicates that the parental Au nanocluster structure remains intact upon Ag binding on the surface, and that the Ag atoms contribute to the overall enhanced absorption.

The initial kinetics of the core-related states of Au₁₅ and Au₁₅@Ag show a rise time in which the Au₁₅@Ag nanocluster is slower. The rise time of the Au₁₅ is convoluted with the instrument's response (110 fs). This difference in the core-related states rise time is not observed in the case of Au₂₅ and Au₂₅@Ag, both of which contain rise times that are masked within the instrument's response. However, for Au₂₅ and Au₂₅@Ag, there is a measureable fast initial decay that is not observed for the smaller nanoclusters. The initial core excited states decay of Au₂₅@Ag is 86 fs faster than that of Au₂₅. This faster initial decay indicates a faster energy transfer within the nanocluster, from the core states to the surface states where the Ag atoms are bound.

The surface-related states between Au and Au@Ag nanoclusters show similar behavior but differ in the initial decay time which depends upon the size of the nanocluster. The kinetic of this ESA fastens by 46% in the bimetallic Au₁₅@Ag nanocluster compared to that of the parental Au₁₅ nanocluster (Table 3). The Au₂₅@Ag shows similar behavior, but the initial decay lifetime only shortens by 15% compared to Au₂₅ (Table 4). The transient absorption spectrum of Ag₁₅ has been reported to have a broad excited state absorption centered at 610 nm with an initial decay lifetime of 146 ps and a second long-lived state.¹⁰ In comparison to this Au₁₅@Ag showed 18% faster decay of ESA lifetime (Table 3) at 600 nm. The transient absorption spectrum of Ag₃₂ has been shown to have three transient features: absorption bleach at 485 nm and two ESA at 651 and 702 nm.¹⁰ The ESA at 651 nm has been shown to have a 470 fs rise time¹⁰ which is and did not show any decay within 1000 ps. The ESA of Au₂₅@Ag is observed to be faster 53% compared to the rise time of ESA of

Ag₃₂. The faster initial decay correlates well with the higher Ag character of the small Au₁₅@Ag nanocluster since Ag nanoclusters have been shown to have lower TPA cross sections due to a faster excited state decay.^{10,67}.

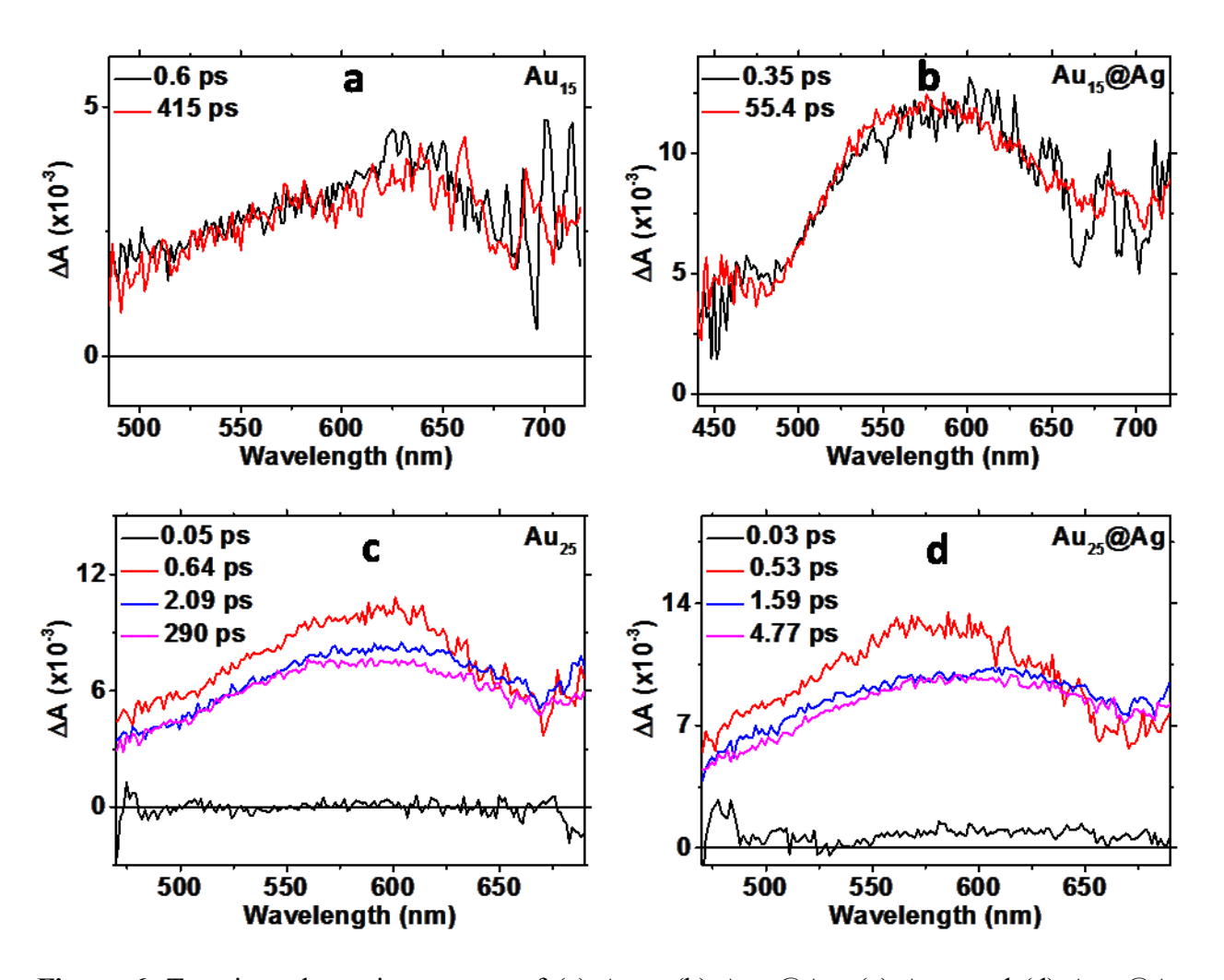


Figure 6. Transient absorption spectra of (a) Au₁₅, (b) Au₁₅@Ag, (c) Au₂₅ and (d) Au₂₅@Ag nanoclusters.

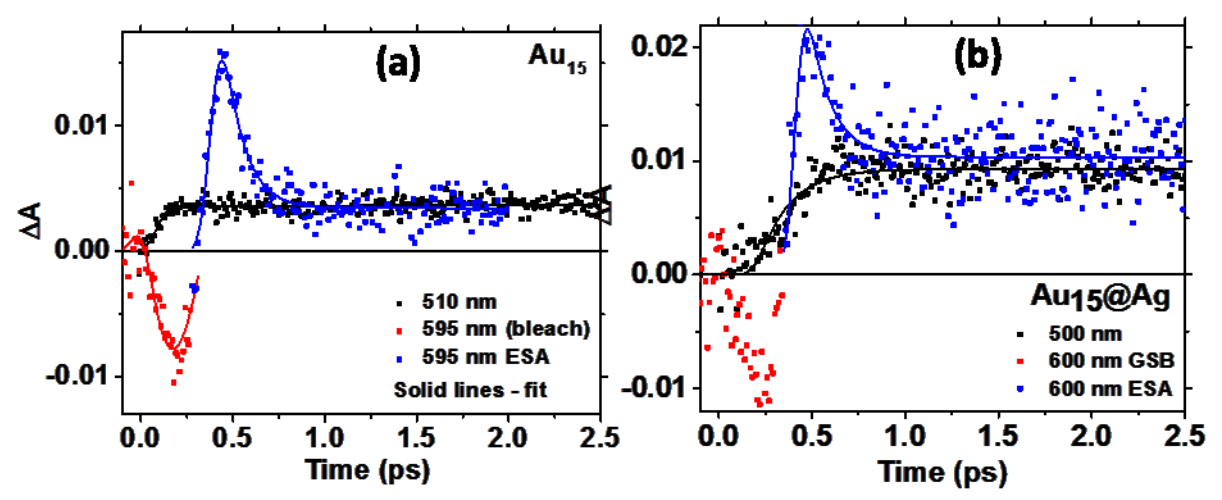


Figure 7. Transient absorption kinetics of Au₁₅ (a) and Au₁₅@Ag (b) nanoclusters.

Table 3. ESA lifetime of Au₁₅ and Au₁₅@Ag

ESA τ (fs)	500 nm		600 nm		
	Au ₁₅	Au ₁₅ @Ag	Au ₁₅	Au ₁₅ @Ag	
t1	inf	166 (rise)	220	119	
t2		Inf	Inf	Inf	

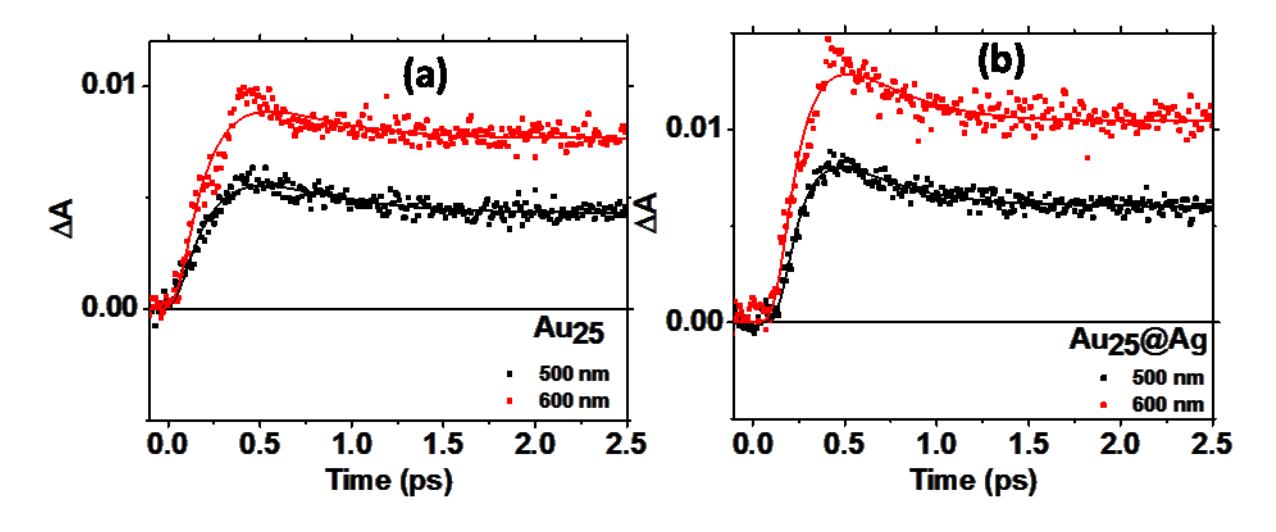


Figure 8. Transient absorption kinetics of Au₂₅ (a) and Au₂₅@Ag (b) nanoclusters.

Table 4. ESA lifetime of Au₂₅ and Au₂₅@Ag

ESA τ (fs)	500 nm		600 nm		
	Au ₂₅	Au ₂₅ @Ag	Au ₂₅	Au ₂₅ @Ag	
t1	281	195	257	219	
t2	Inf	Inf	Inf	Inf	

The fluorescence of gold nanoclusters has also been explored in longer nanosecond to microsecond time scales using time-correlated single photon counting. 64,65, 70-72 The fluorescence decay of bovine serum albumin (BSA)-protected Au₂₅ nanocluster has been the most thoroughly investigated with two observed components: a fast nanosecond and a long microsecond component. 70 Wen et al. proposed that the fast nanosecond component is due to prompt fluorescence, and the long microsecond component is due to delayed fluorescence.⁷⁰ The faster nanosecond component is more dominant in the shorter wavelengths around 550 nm with a decay constant of 1.2 ns. 70 The long microsecond component, dominant in longer wavelengths ~650 nm, has been more widely measured and verified by several other studies with the decay constant ranging from 1.2 µs to 1.88 µs. 64,65,70-72 The delay fluorescence arises from a high probability of intersystem crossing from singlet to triplet and subsequently, reverse intersystem crossing from triplet to singlet states. Delayed fluorescence of the Au₂₅ nanocluster has been correlated to the Au(I)-S semirings in the protecting surface states. ^{70,73}This result is confirmed by the BSA-protected Au₈ nanocluster which does not have Au(I)-S semiring motif and exhibits no long lifetime component.⁷³ The formation of the triplet state is due to the d¹⁰ electronic structure of the Au(I)-S complex which induces ligand-localized and ligand-to-metal charge transfer. 74 Other groups have also explored the long decay component of the Au₂₅ nanocluster resulting in decay constants of 1.24 µs to 2.3 µs. 63,75 No other mechanisms have been proposed for the short and long decay in the nanosecond to microsecond regime. Silver nanoclusters resemble their gold counterparts with a discrete number of silver atoms in the core protected by a silver-ligand protective shell.⁹ Fluorescence of Ag nanoclusters originates from the silver-ligand interface and exhibit emission at 650 nm. Ag₃₂(SG)₁₉ and Ag₁₅(SG)₁₁ possessed decay lifetimes of 130 ps at 650 nm, much longer than gold nanoclusters due to weak coupling to Ag 4d electrons.¹⁰ Ag nanoclusters, however, are not as stable as their gold counterparts despite their greater fluorescence properties.

As can be seen from Figure 8 the femtosecond transient kinetics of the Au and Au@Ag nanoclusters do not decay within the measured timeframe. Particularly Au₂₅ and Au₂₅@Ag showed long decay kinetics (Figure 8b). Recently, Zhou et. al.⁷⁶ through a combine femtosecond and nanosecond transient absorption measurements, have demonstrated that the 8-electron CdAu₂₄(SR)₁₈ and HgAu₂₄(SR)₁₈ show a long excited state lifetime (50-200ns) along with a weak picosecond relaxation. The authors have shown that the number of valence electrons plays a crucial role in determining the excited dynamics of metal doped Au₂₅ nanoclusters.⁷⁶ Hence, to shed more light on the excited state dynamics of the Au@Ag nanoclusters, nanosecond transient absorption spectroscopic technique has been employed.

The nanosecond transient absorption kinetics were recorded for Au₂₅ and Au₂₅@Ag nanoclusters at 500nm and 600nm. Excited state absorption decay profiles monitored at 500nm and 600nm and the corresponding transient lifetimes for Au₂₅ and Au₂₅@Ag are shown in Figure 9. The excited state absorption peak for Au₂₅@Ag is observed at ~600 nm, whereas Au₂₅ shows an ESA peak at ~500 nm (Figure 10, 11). It is interesting to note from our result that the ESA lifetime of Au₂₅@Ag (797 ns) at 600nm has been observed to be enhanced by ~3 times the ESA lifetime of Au₂₅ (252 ns, Figure 9b). A small increase in the transient lifetime has also been observed at 500 nm for Au₂₅@Ag (454 ns) than that of Au₂₅ (Figure 9a). However, the effect is observed to be more pronounced at 600 nm. Such a long ESA lifetime for Au₂₅@Ag certainly points out the contribution of Ag on the dynamics of the surface states of the nanocluster. Another interesting observation is the red shift in the transient spectrum for Au₂₅@Ag (around 600 nm) compared to that of Au₂₅ (around 500 nm). Zhou et. al., through nanosecond transient absorption measurements, have shown that the excited state lifetimes for [Au₂₅], CdAu₂₄ and HgAu₂₄ were 100, 200 and 50 ns respectively. And they correlated their time-resolved observations to the optical bandgaps for the three nanoclusters. 76 They suggested that the trend of excited state lifetimes follows the bandgap law, i.e. higher the bandgap, the longer the excited state lifetime.⁷⁷ By comparing their relaxation dynamics data of Cd/Hg doped Au₂₅ clusters with data of Pd/Pt

doped Au₂₅ nanoclusters, ^{77,78} the authors have found that the CdAu₂₄ and HgAu₂₄ (8-electron configuration) are similar to anionic Au₂₅ (8-electron configuration).⁷⁷ Similarly, relaxation dynamics of Pd/Pt doped Au₂₅ clusters (6-electron system) was suggested to be more like the neutral Au₂₅ (7-electron system).⁷⁶ Hence they concluded that the number of valence electrons has a significant role on excited state dynamics on metal doped nanoclusters.⁷⁶ Another report by Ramakrishna and Coworkers, 79 through steady-state absorption and voltammetry measurements, demonstrates the effect of Pt and Hg doping in Au₂₅ nanoclusters. The authors have shown that Pt-doping drastically decreases the HOMO-LUMO gap by virtue of being a six electron system, whereas Hg doping of Au₂₅ doesn't affect the HOMO-LUMO gap.⁷⁹ In our present study, the increased excited state lifetime of Au₂₅@Ag (Figure 9b) compared to the Au₂₅ clearly points out to the fact that Au₂₅@Ag follow the energy gap law as silver doping has been shown to increase the HOMO-LUMO gap in Ag doped Au nanoclusters. 52 This is in accordance to the reported suggestions shown for CdAu₂₄, HgAu₂₄ and PtAu₂₄ by Zhou et. al. ⁷⁶ and Ramakrishna and coworkers ⁷⁹ A closer look into the nanosecond transient absorption (ns-TA) data of Au₂₅, and HgAu₂₄ by Zhou et. al. 76, indicates a small blue shift in ESA spectrum for HgAu₂₄ (centered around 580 nm) compared to Au₂₅ (centered around 610 nm) while the optical bandgap of both Au₂₅ and HgAu₂₄ are comparable. ⁷⁶ In comparison to this we have observed a red shift in the transient absorption spectra for Au₂₅@Ag compared to the Au₂₅ nanocluster. Our observation can be rationalized by taking into consideration the dopant occupying site in a bimetallic nanocluster. In Cd, Hg and Pt doped Au₂₅, the dopant occupies the center core site^{76,79} where as in our present study, in A25@Ag, Ag atoms occupy the staple motif which can affect the absorption properties of the surface states. Recent theoretical study by Kacprzak et. al. on PdAu₂₄(SR)₁₈²⁻ demonstrates that the optical absorption and the HOMO–LUMO gap depend sensitively on the site of the doping Pd atom. 80 For example the HOMO-LUMO gap is shown to increase when Pd occupies the center doping position whereas the core surface and ligand shell doping positions showed considerably lower HOMO-LUMO gaps. 80 A red shift in the optical absorption spectra of the aromatic monolayer protected clusters Au_{36-x}Ag_x(SPh-tBu)₂₄, has also been observed by Dass and coworkers.⁸¹ The authors have attributed such observation towards the effect of conjugation between Ag in the staples and the aromatic residue in the thiolate group. 81 In another study, Xiang et. al. have determined

the structure of Au₁₅Ag₃(SC₆H₁₁)₁₄ through X-ray crystallography and analysed the optical absorption spectra through density functional theory (DFT).⁸² The authors have pointed out that the blue shift in the HOMO-LUMO transition in the Ag doped nanoclusters compared to its Au₁₈ counterpart, is due to the stronger sd hybridization and the lower 6s orbital energy of Au atoms.⁸²

Based on the above discussion, we can infer that the position of the doping metal in a bimetallic nanocluster can significantly influence the HOMO-LUMO gap which in turn can change their photophysical properties. The above discussion points out that the position of the Ag atom in the Au@Ag nanoclusters can significantly influence the optical properties of the bimetallic nanoclusters. The fact that, in our bimetallic nanoclusters under investigation, the Ag atom doesn't displace any Au atom and simply occupies the staple motif, can be reasoned behind the observed red shift in the transient absorption spectra of $Au_{25}@Ag$ nanocluster compared to that of Au_{25} .

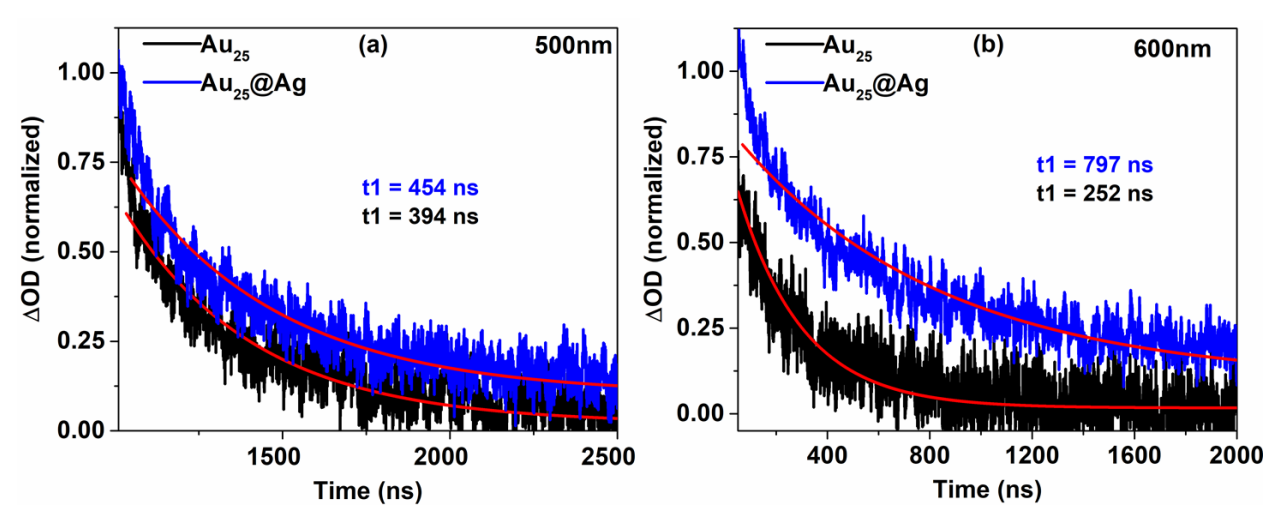


Figure 9. Nanosecond transient absorption decay profiles of Au₂₅ and Au₂₅@Ag. Single exponential fit to the data points are shown as red lines.

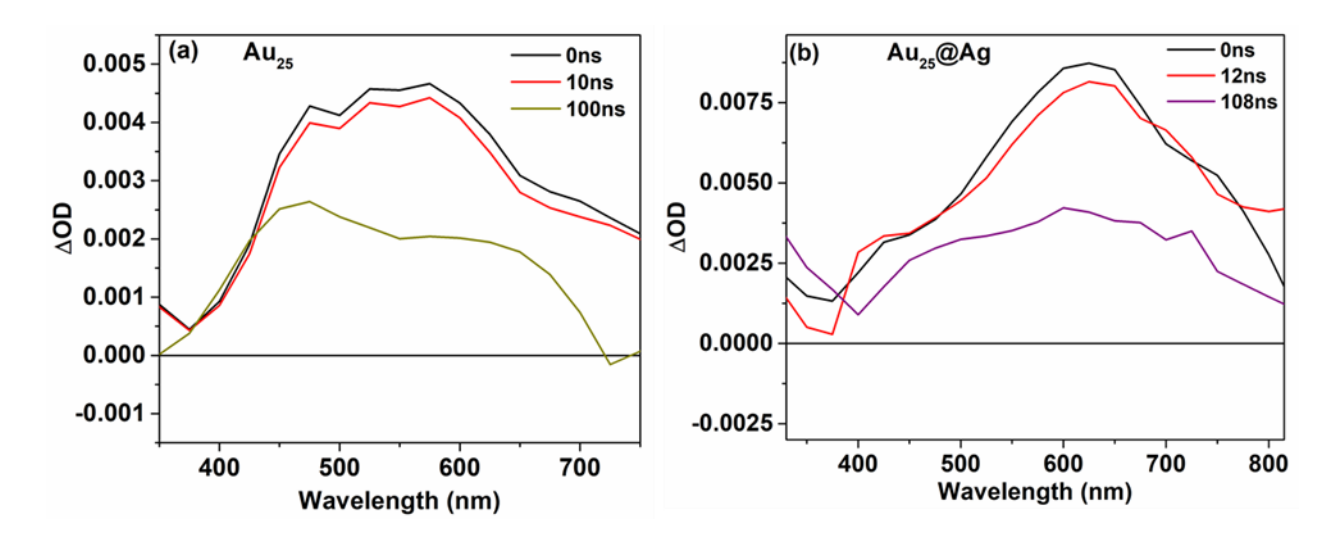


Figure 10. Nanosecond transient absorption spectra of Au₂₅ and Au₂₅@Ag.

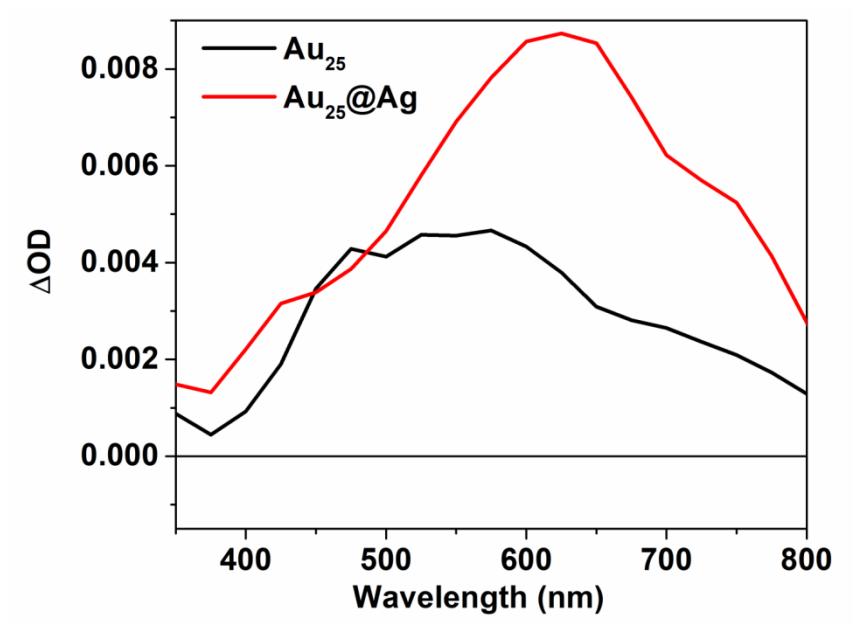


Figure 10. Nanosecond transient absorption spectra of Au₂₅ and Au₂₅@Ag showing red shift in the absorption spectra of Au₂₅@Ag.

V. CONCLUSION

The present work demonstrates the effect of silver doping on the structure and optical properties of Au₁₅@Ag, Au₁₈@Ag and Au₂₅@Ag nanoclusters. The bimetallic Au@Ag nanoclusters showed stronger absorption compared to the parental Au nanoclusters. Particularly the peak at 350 nm is observed to be more pronounced in Au@Ag nanoclusters

which indicates the presence of Ag⁺ ion in the staple motif as no significant shift has been observed in the absorption which would indicate Ag doping in the Au nanocluster's core. The increase in Ag character of the bimetallic nanoclusters is also evidenced by the emission blue shift towards 650 nm which is typical for Ag nanoclusters. This behavior indicates the formation of S-Ag-S bonds in the staple motifs of the Au nanoclusters, that masks the fluorescence originating from S-Au-S staples. It is observed that the spectral shift is greater in the smaller nanocluster Au₁₅@Ag, due to the higher ratio of Ag atoms on the staple motif than to the Au atoms in the core. The excited states dynamics of the nanoclusters contain a long lifetime component which was measured to be longer in the bimetallic nanocluster compared to the Au nanocluster. Although Ag nanoclusters have been shown to have lower two-photon absorption cross sections compared to Au nanoclusters, as it is noted between the Au₁₅@Ag and Au₁₈@Ag nanoclusters, the molecular symmetry is the determining factor for the cross-section enhancement in the Au₂₅@Ag nanocluster. Femtosecond transient absorption spectroscopic study revealed a faster excited state absorption (ESA) kinetics of the Au₁₅@Ag which can be correlated with the higher Ag character of the small Au₁₅@Ag. Nanosecond transient absorption measurements revealed a significant difference in ESA kinetics of Au₂₅@Ag and Au₂₅ with a red shift in the ESA spectra of Au₂₅@Ag. Therefore, bimetallic nanoclusters present a way to combine properties that arise from their constituents. The Au@Ag nanoclusters offer enhanced optical properties due to the Ag atoms while obtaining colloidal stability that is characteristic of Au nanoclusters.

ASSOCIATED CONTENT

Supporting Information

Steady state fluorescence spectra of the Au and Au@Ag nanoclusters under investigation have been provided.

AUTHOR INFORMATION

Corresponding author

*tgoodson@umich.edu

ACKNOWLEDGEMENT

This work is supported by.......PKS thanks Indo-US Science and Technology Forum for SERB Indo-US Postdoctoral fellowship.

REFERENCES

- (1) Qian, H.; Zhu, M.; Wu, Z.; Jin, R. Quantum Sized Gold Nanoclusters with Atomic Precision. *Acc. Chem. Res.* **2012**, *45*, 1470-1479.
- (2) Zeng, C.; Chen, Y.; Iida, K.; Nobusada, K.; Kirschbaum, K.; Lambright, K. J.; Jin, R. Gold Quantum Boxes: On the Periodicities and the Quantum Confinement in the Au28, Au₃₆, Au₄₄, and Au₅₂ Magic Series. *J. Am. Chem. Soc.* 2016, 138, 3950-3953.
- (3) Yau, S. H.; Varnavski, O.; Goodson III, T. An Ultrafast Look at Au Nanoclusters. *Acc. Chem. Res.* **2013**, *46*, 1506–1516.
- (4) Negishi, Y.; Nakazaki, T.; Malola, S.; Takano, S.; Niihori, Y.; Kurashige, W.; Yamazoe, S.; Tsukuda, T.; Häkkinen, H. A Critical Size for Emergence of Nonbulk Electronic and Geometric Structures in Dodecanethiolate-Protected Au Clusters. *J. Am. Chem. Soc.* **2015**, *137*, 1206-1212.
- (5) Russier-Antoine, I.; Bertorelle, F.; Vojkovic, M.; Rayane, D.; Salmon, E.; Jonin, C.; Dugourd, P.; Antoine, R.; Brevet, P.-F. Non-linear Optical Properties of Gold Quantum Clusters. The Smaller The Better. *Nanoscale* **2014**, *6*, 13572-13578.
- (6) Philip, R.; Chantharasupawong, P.; Qian, H.; Jin, R.; Thomas, J. Evolution of Nonlinear Optical Properties: From Gold Atomic Clusters to Plasmonic Nanocrystals. *Nano Lett.* 2012, 12, 4661-4667.
- (7) Varnavski, O.; Ramakrishna, G.; Kim, J.; Lee, D.; Goodson III, T. Critical Size for the Observation of Quantum Confinement in Optically Excited Gold Clusters. *J. Am. Chem. Soc.* **2010**, *132*, 16.
- (8) Jin, R. Atomically Precise Metal Nanoclusters: Stable Sizes and Optical Properties. *Nanoscale* **2015**, *7*, 1549-1565.
- (9) Ashenfelter, B. A.; Desireddy, A.; Yau, S. H.; Goodson III, T.; Bigioni, T. P.

- Fluorescence from Molecular Silver Nanoparticles. *J. Phys. Chem. C* **2015**, *119*, 20728-20734.
- (10) Yau, S. H.; Ashenfelter, B.; Desireddy, A.; Ashwell, A. P.; Varnavski, O.; Schatz, G. C.; Bigioni, T.; Goodson III, T. Optical Properties and Structural Relationships of the Silver Nanoclusters Ag₃₂(SG)₁₉ and Ag₁₅(SG)₁₁. *J. Phys. Chem. C* **2017**, *121*, 1349-1361.
- (11) Zhu, M.; Aikens, C. M.; Hollander, F. J.; Schatz, G. C.; Jin, R. Correlating the Crystal Structure of A Thiol-Protected Au 25 Cluster and Optical Properties. *J. Am. Chem. Soc.* 2008, 130, 5883–5885.
- (12) Aikens, C. M. Origin of Discrete Optical Absorption Spectra of M₂₅(SH)₁₈ Nanoparticles (M = Au, Ag). *J. Phys. Chem. C* **2008**, *112* (50), 19797-19800.
- (13) Heaven, M. W.; Dass, A.; White, P. S.; Holt, K. M.; Murray, R. W. Crystal Structure of the Gold Nanoparticle [N(C₈H₁₇)₄][Au₂₅(SCH₂CH₂Ph)₁₈]. *J. Am. Chem. Soc.* **2008**, *130*, 3754-3755.
- (14) Akola, J.; Walter, M.; Whetten, R. L.; Häkkinen, H.; Grönbeck, H. On the Structure of Thiolate-Protected Au₂₅. *J. Am. Chem. Soc.* **2008**, *130*, 3756-3757.
- Yau, S. H.; Varnavski, O.; Gilbertson, J. D.; Chandler, B.; Ramakrishna, G.; Goodson III,
 T. Ultrafast Optical Study of Small Gold Monolayer Protected Clusters: A Closer Look at Emission. *J. Phys. Chem. C* 2010, *114*, 15979.
- (16) Yau, S. H.; Abeyasinghe, N.; Orr, M.; Upton, L.; Varnavski, O.; Werner, J. H.; Yeh, H.-C.; Sharma, J.; Shreve, A. P.; Martinez, J. S.; Goodson III, T. Bright Two-Photon Emission and Ultra-Fast Relaxation Dynamics in A DNA-Templated Nanocluster Investigated by Ultra-Fast Spectroscopy. *Nanoscale* 2012, 4, 4247-4254.
- (17) Devadas, M. S.; Kim, J.; Sinn, E.; Lee, D.; Goodson III, T.; Ramakrishna, G. Unique Ultrafast Visible Luminescence in Monolayer-Protected Au₂₅ Clusters. *J. Phys. Chem. C* **2010**, *114*, 22417-22423.
- (18) Link, S.; Beeby, A.; FitzGerald, S.; El-Sayed, M. A.; Schaaff, T. G.; Whetten, R. Visible to Infrared Luminescence from a 28-Atom Gold Cluster. *J. Phys. Chem. B* **2002**, *106*, 3410-3415.

- (19) Wu, Z.; Wang, M.; Yang, J.; Zheng, X.; Cai, W.; Meng, G.; Qian, H.; Wang, H.; Jin, R. Well-Defined Nanoclusters as Fluorescent Nanosensors: A Case Study on Au₂₅(SG)₁₈. Small 2012, 8, 2028-2035.
- (20) Abeyasinghe, N.; Kumar, S.; Sun, K.; Mansfield, J. F.; Jin, R.; Goodson III, T. Enhanced Emission from Single Isolated Gold Quantum Dots Investigated Using Two-Photon-Excited Fluorescence Near-Field Scanning Optical Microscopy. *J. Am. Chem. Soc.* **2016**, *138*, 16299-16307.
- (21) Polavarapu, L.; Manna, M.; Xu, Q.-H. Biocompatible Glutathione Capped Gold Clusters as One- and Two-Photon Excitation Fluorescence Contrast Agents for Live Cells Imaging. *Nanoscale* **2011**, *3*, 429-434.
- (22) Shang, L.; Dong, S.; Nienhaus, G. U. Ultra-Small Fluorescent Metal Nanoclusters: Synthesis and Biological Applications. *Nano Today* **2011**, *6*, 401-418.
- (23) Ho-Wu, R.; Yau, S. H.; Goodson III, T. Efficient Singlet Oxygen Generation in Metal Nanoclusters for Two-Photon Photodynamic Therapy Applications. *J. Phys. Chem. B* **2017**, *121*, 10073-10080.
- (24) Qu, X.; Li, Y.; Li, L.; Wang, Y.; Liang, J.; Liang, J. Fluorescent Gold Nanoclusters: Synthesis and Recent Biological Application. *J. Nanomater.* **2015**, *2015*, 1–23.
- (25) Bain, D.; Paramanik, B.; Patra, A. Silver(I)-Induced Conformation Change of DNA: Gold Nanocluster as a Spectroscopic Probe. *J. Phys. Chem. C* **2017**, *121*, 4608–4617.
- (26) Paramanik, B.; Bain, D.; Patra, A. Making and Breaking of DNA-Metal Base Pairs: Hg²⁺ and Au Nanocluster Based Off/On Probe. *J. Phys. Chem. C* **2016**, *120*, 17127–17135
- (27) He, F.; Feng, L.; Yang, P.; Liu, B.; Gai, S.; Yang, G.; Dai, Y.; Lin, J. Enhanced Up/down-Conversion Luminescence and Heat: Simultaneously Achieving in One Single Core-Shell Structure for Multimodal Imaging Guided Therapy. *Biomaterials* **2016**, *105*, 77–88.
- (28) Miao, Z.; Hou, W.; Liu, M.; Zhang, Y.; Yao, S. BSA Capped Bi-Functional Fluorescent Cu Nanoclusters as pH Sensor and Selective Detection of Dopamine. *New J. Chem. New J. Chem.* 2018, 42, 1446–1456.

- (29) Naaz, S.; Chowdhury, P. Sunlight and Ultrasound-Assisted Synthesis of Photoluminescent Silver Nanoclusters: A Unique "Knock Out" Sensor for Thiophilic Metal Ions. *Sensors Actuators B. Chem.* **2017**, *241*, 840–848.
- (30) Ding, C.; Tian, Y. Gold Nanocluster-Based Fluorescence Biosensor for Targeted Imaging in Cancer Cells and Ratiometric Determination of Intracellular pH. *Biosens. Bioelectron.* 2015, 65, 183-190.
- (31) Biswas, A.; Banerjee, S.; Gart, E. V.; Nagaraja, A. T.; McShane, M. J. Gold Nanocluster Containing Polymeric Microcapsules for Intracellular Ratiometric Fluorescence Biosensing. *ACS Omega* **2017**, *2*, 2499-2506.
- (32) Li, G.; Jin, R. Atomically Precise Gold Nanoclusters as New Model Catalysts. *Acc. Chem. Res.* **2013**, *27*, 1749–1758.
- (33) Fang, J.; Zhang, B.; Yao, Q.; Yang, Y.; Xie, J.; Yan, N. Recent Advances in the Synthesis and Catalytic Applications of Ligand Protected, Atomically Precise Metal Nanoclusters. *Coordination Chemistry Reviews* **2016**, *322*, 1–29.
- (34) Daniel, M.-C.; Astruc, D. Gold Nanoparticles: Assembly, Supramolecular Chemistry, Quantum-Size-Related Properties, and Applications toward Biology, Catalysis, and Nanotechnology. *Chem. Rev.* 2004, 104, 293–346.
- (35) Luo, Z.; Yuan, X.; Yu, Y.; Zhang, Q.; Leong, D. T.; Lee, J. Y.; Xie, J. From Aggregation-Induced Emission of Au(I)—Thiolate Complexes to Ultrabright Au(0)@Au(I)—Thiolate Core—Shell Nanoclusters. *J. Am. Chem. Soc.* **2012**, *134*, 16662-166670.
- (36) Li, B.; Wang, X.; Shen, X.; Zhu, W.; Xu, L.; Zhou, X. Aggregation-Induced Emission from Gold Nanoclusters for Use As A Luminescence-Enhanced Nanosensor to Detect Trace Amounts of Silver Ions. *J. Colloid Interface Sci.* **2016**, *467*, 90-96.
- (37) Dou, X.; Yuan, X.; Yu, Y.; Luo, Z.; Yao, Q.; Leong, D. T.; Xie, J. Lighting Up Thiolated Au@Ag Nanoclusters Via Aggregation-Induced Emission. *Nanoscale* **2014**, *6*, 157-161.
- (38) Wu, Z.; Jin, R. On the Ligand's Role in the Fluorescence of Gold Nanoclusters. *Nano Lett.* **2010**, *10*, 2568-2573.

- (39) Zhou, Q.; Lin, Y.; Xu, M.; Gao, Z.; Yang, H.; Tang, D. Facile Synthesis of Enhanced Fluorescent Gold–Silver Bimetallic Nanocluster and Its Application for Highly Sensitive Detection of Inorganic Pyrophosphatase Activity. *Anal. Chem.* **2016**, *88*, 8886-8892.
- (40) Wang, S.; Meng, X.; Das, A.; Li, T.; Song, Y.; Cao, T.; Zhu, X.; Zhu, M.; Jin, R. A 200-Fold Quantum Yield Boost in The Photoluminescence of Silver-Doped Ag_(x)Au_(25-x)
 Nanoclusters: The 13th Silver Atom Matters. *Angew. Chem. Int. Ed. Engl.* **2014**, *53*, 2376-2380.
- (41) Yu, Y.; Luo, Z.; Chevrier, D. M.; Leong, D. T.; Zhang, P.; Jiang, D.; Xie, J. Identification of a Highly Luminescent Au₂₂(SG)₁₈ Nanocluster. *J. Am. Chem. Soc.* **2014**, *136*, 1246-1249.
- (42) Yang, H.; Lei, J.; Wu, B.; Wang, Y.; Zhou, M.; Xia, A.; Zheng, L.; Zheng, N. Crystal Structure of A Luminescent Thiolated Ag Nanocluster With an Octahedral Ag₆ ⁴⁺ core. *Chem. Commun.* **2013**, *49*, 300-302.
- (43) Negishi, Y.; Iwai, T.; Ide, M. Continuous Modulation of Electronic Structure of Stable Thiolate-Protected Au₂₅ Cluster by Ag Doping. *Chem. Commun.* **2010**, *46*, 4713-4715.
- (44) Choi, J.-P.; Fields-Zinna, C. A.; Stiles, R. L.; Balasubramanian, R.; Douglas, A. D.; Crowe, M. C.; Murray, R. W. Reactivity of [Au₂₅(SCH₂CH₂Ph)₁₈]¹⁻ Nanoparticles with Metal Ions. *J. Phys. Chem. C* **2010**, *114*, 15890-15896.
- (45) Wu, Z. Anti-Galvanic Reduction of Thiolate-Protected Gold and Silver Nanoparticles. *Angew. Chemie Int. Ed.* **2012**, *51*, 2934-2938.
- (46) Yao, Q.; Feng,Y.; V. Fung, Yu,Y.; Jiang, D.-e.; Yang, J.; Xie, J. Precise Control of Alloying Sites of Bimetallic Nanoclusters via Surface Motif Exchange Reaction. *Nat. Commun.* **2017**, *8*, 1555.
- (47) Jiang, D.-E.; Overbury, S. H.; Dai, S. Structure of Au₁₅(SR)₁₃ and Its Implication for the Origin of the Nucleus in Thiolated Gold Nanoclusters. *J. Am. Chem. Soc.*, **2013**, *135*, 8786–8789.
- (48) Chen, S.; Wang, S.; Zhong, J.; Song, Y.; Zhang, J.; Sheng, H.; Pei, Y.; Zhu, M. The Structure and Optical Properties of the [Au₁₈(SR)₁₄] Nanocluster. *Angew. Chemie Int. Ed.*

- **2015**, *54*, 3145-3149.
- (49) Das, A.; Liu, C.; Byun, H. Y.; Nobusada, K.; Zhao, S.; Rosi, N.; Jin, R. Structure Determination of [Au₁₈(SR)₁₄]. *Angew. Chemie Int. Ed.* **2015**, *54*, 3140-3144.
- (50) Tlahuice-Flores, A.; Jose-Yacama'n, M.; Whetten, L. R. On the Structure of the Thiolated Au₁₅ Cluster. *Phys. Chem. Chem. Phys.*, **2013**, *15*, 19557—19560.
- (51) Conn, B. E.; Atnagulov, A.; Yoon, B.; Barnett, R. N.; Landman, U.; Bigioni, T. P. Confirmation of A De Novo Structure Prediction For An Atomically Precise Monolayer-Coated Silver Nanoparticle. *Sci. Adv.* **2016**, *2*, e1601609(1-7).
- (52) Guidez, E. B.; Makinen, V.; Hakkinen, H.; Aikens, C. M. Effects of Silver Doping on the Geometric and Electronic Structure and Optical Absorption Spectra of the Au_{25-n}Ag_n(SH)₁₈- (n = 1, 2, 4, 6, 8, 10, 12) Bimetallic Nanoclusters. *J. Phys. Chem. C* **2012**, 116, 20617-20624.
- (53) Ramakrishna, G.; Varnavski, O.; Kim, J.; Lee, D.; Goodson III, T. Quantum-Sized Gold Clusters as Efficient Two-Photon Absorbers. *J. Am. Chem. Soc.* **2008**, *130*, 5032-5033.
- (54) Kawasaki, H.; Kumar, S.; Li, G.; Zeng, C.; Kauffman, D. R.; Yoshimoto, J.; Iwasaki, Y.; Jin, R. Generation of Singlet Oxygen by Photoexcited Au₂₅(SR)₁₈ Clusters. *Chem. Mater.* 2014, 26, 2777-2788.
- (55) Shibu, E. S.; Muhammed, M. A. H.; Tsukuda, T.; Pradeep, T. Ligand Exchange of Au₂₅SG₁₈ Leading to Functionalized Gold Clusters: Spectroscopy, Kinetics, and Luminescence. *J. Phys. Chem. C* **2008**, *112*, 12168-12176.
- (56) Roduner, E. Size Matters: Why Nanomaterials Are Different. *Chem. Soc. Rev.*, **2006**, 35, 583–592.
- (57) Negishi, Y.; Nobusada, K.; Tsukuda, T. Glutathione-Protected Gold Clusters Revisited: Bridging the Gap between Gold(I)-Thiolate Complexes and Thiolate-Protected Gold Nanocrystals.
- (58) Kurashige, W.; Niihori, Y.; Sharma, S.; Negishi, Y. Recent Progress in the Functionalization Methods of Thiolate- Protected Gold Clusters. *J. Phys. Chem.*

- Lett., 2014, 5, 4134-4142.
- (59) Russier-Antoine, I.; Bertorelle, F.; Vojkovic, M.; Rayane, D.; Salmon, E.; Jonin, C.; Dugourd, P.; Antoine, R.; Brevet, P.-F. Non-Linear Optical Properties of Gold Quantum Clusters. The Smaller the Better. *Nanoscale* **2014**, *6*.
- (60) Varnavski, O.; Ramakrishna, G.; Kim, J.; Lee, D.; Goodson, T. Critical Size for the Observation of Quantum Confinement in Optically Excited Gold Clusters.
- (61) Zhou, M.; Zeng, C.; Chen, Y.; Zhao, S.; Sfeir, M. Y.; Zhu, M.; Jin, R. Evolution from the Plasmon to Exciton State in Ligand-Protected Atomically Precise Gold Nanoparticles. *Nat. Commun.* 2016, 7.
- (62) Wu, Z.; Gayathri, C.; Gil, R. R.; Jin, R. Probing the Structure and Charge State of Glutathione-Capped Au ₂₅ (SG) ₁₈ Clusters by NMR and Mass Spectrometry. *J. Am. Chem. Soc.*, **2009**, *131*, 6535–6542.
- (63) Milowska, K. Z.; Stolarczyk, J. K.; Daniel, M.-C.; Astruc, D.; Jin, R.; Fernando, A.; Dimuthu, K. L.; Weerawardene, M.; Karimova, N. V.; Aikens, C. M.; et al. Role of Ligand-ligand vs. Core-core Interactions in Gold Nanoclusters. Phys. Chem. Chem. Phys. 2016, 18, 12716–12724.
- (64) Pyo, K.; Thanthirige, V. D.; Yoon, S. Y.; Ramakrishna, G.; Lee, D. Enhanced Luminescence of Au₂₂(SG)₁₈ Nanoclusters via Rational Surface Engineering. *Nanoscale* **2016**, 8.
- (65) Shi, J.; Cooper, J. K.; Lindley, S.; Williams, O.; Kliger, D. S.; Xu, Y.; Bao, Y.; Zhang, J. Z. The Excited State Dynamics of Protein-Encapsulated Au Nanoclusters. *Chem. Phys. Lett.* 2014, 610–611, 125–130.
- (66) Yu, P.; Wen, X.; Toh, Y.-R.; Huang, J.; Tang, J. Metallophilic Bond-Induced Quenching of Delayed Fluorescence in Au ₂₅ @BSA Nanoclusters. *Part. Part. Syst. Charact.* **2013**, 30, 467–472.
- (67) Sanader, Ž.; Krstić, M.; Russier-Antoine, I.; Bertorelle, F.; Dugourd, P.; Brevet, P.-F.; Antoine, R.; Bonačić-Koutecký, V. Two-Photon Absorption of Ligand-Protected Ag₁₅ Nanoclusters. Towards A New Class of Nonlinear Optics Nanomaterials. *Phys. Chem.*

- Chem. Phys. 2016, 18, 12404-12408.
- (68) Bhaskar, A.; Guda, R.; Haley, M. M.; Goodson, T. Building Symmetric Two-Dimensional Two-Photon Materials. *J. Am. Chem. Soc.* **2006**, *128*, 13972-13973.
- (69) Varnavski, O. P.; Goodson Iii, T.; Mohamed, M. B.; El-Sayed, M. A. Femtosecond Excitation Dynamics in Gold Nanospheres and Nanorods. *Phys. Rev. B* **2005**, *72*, 235405.
- (70) Wen, X.; Yu, P.; Toh, Y.-R.; Hsu, A.-C.; Lee, Y.-C.; Tang, J. Fluorescence Dynamics in BSA-Protected Au ₂₅ Nanoclusters. *J. Phys. Chem. C*, **2012**, *116*, 19032–19038.
- (71) Raut, S.; Chib, R.; Rich, R.; Shumilov, D.; Gryczynski, Z.; Gryczynski, I. Polarization Properties of Fluorescent BSA Protected Au 25 Nanoclusters. *Nanoscale*, **2013**,*5*, 3441-3446.
- (72) Mali, B.; Dragan, A. I.; Karolin, J.; Geddes, C. D. Photophysical Characterization and α-Type Delayed Luminescence of Rapidly Prepared Au Clusters. J. Phys. Chem. C, 2013, 117, 16650–16657.
- (73) Wen, X.; Yu, P.; Toh, Y.-R.; Ma, X.; Huang, S.; Tang, J. Fluorescence Origin and Spectral Broadening Mechanism in Atomically Precise Au₈ Nanoclusters. *Nanoscale*, **2013**,*5*, 10251-10257.
- (74) Wang, X.-Y.; Guerzo, A. Del; Schmehl, R. H. Photophysical Behavior of Transition Metal Complexes Having Interacting Ligand Localized and Metal-to-Ligand Charge Transfer States. *J. Photochem. Photobiol. C Photochem. Rev.* **2004**, *5*, 55–77.
- (75) Yahia-Ammar, A.; Sierra, D.; Meola, F.; Hildebrandt, N.; Le Gueel, X. Self-Assembled Gold Nanoclusters for Bright Fluorescence Imaging and Enhanced Drug Delivery. *ACS Nano*, **2016**, *10*, 2591–2599.
- (76) Zhou, M.; Yao, C.; Sfeir, M. Y.; Higaki, T.; Wu, Z.; Jin, R. Excited-State Behaviors of M₁Au₂₄(SR)₁₈ Nanoclusters: The Number of Valence Electrons Matters. *J. Phys. Chem. C*, **2018**, *122*, 13435–13442.
- (77) Zhou, M.; Qian, H.; Sfeir, M. Y.; Nobusadac, K.; Jin, R. Effects of Single Atom Doping on The Ultrafast Electron Dynamics of M₁Au₂₄(SR)₁₈ (M = Pd, Pt) Nanoclusters. *Nanoscale*, **2016**, 8, 7163–7171.

- (78) Qian, H.; Sfeir, M. Y.; Jin, R. Ultrafast Relaxation Dynamics of [Au₂₅(SR)18]^q
 Nanoclusters: Effects of Charge State. *J. Phys. Chem. C* **2010**, *114*, 19935 19940.
- (79) Thanthirige, V. D.; Kim, M.; Choi, W.; Kwak, K.; Lee, D.; Ramakrishna, G. Temperature-Dependent Absorption and Ultrafast Exciton Relaxation Dynamics in MAu₂₄(SR)₁₈Clusters (M = Pt, Hg): Role of the Central Metal Atom. J. Phys. Chem. C 2016, 120, 23180 23188.
- (80) Kacprzak, K. A.; Lehtovaara, L.; Akola, J.; Lopez-Acevedoa, O.; Ha¨kkinen, H. A Density Functional Investigation of Thiolate-Protected Bimetal PdAu₂₄(SR)₁₈ Z Clusters: Doping The Superatom Complex. *Phys. Chem. Chem. Phys.*, **2009**, *11*, 7123–7129.
- (81) Theivendran, S.; Chang, L.; Mukherjee, A.; Sementa, L.; Stener, M.; Fortunelli, A.; Dass, A. Principles of Optical Spectroscopy of Aromatic Alloy Nanomolecules: Au_{36-x}Ag_x(SPh-tBu)₂₄. J. Phys. Chem. C 2018, 122, 4524–4531.
- (82) Xiang, J.; Li, P.; Song, Y.; Liu, X.; Chong, H.; Jin, S.; Pei, Y.; Yuana X.; Zhu, M. X-Ray Crystal Structure, and Optical and Electrochemical Properties of the Au₁₅Ag₃(SC₆H₁₁)₁₄ Nanocluster with A Core–Shell Structure. *Nanoscale*, **2015**, 7, 18278–18283.